Research Square

Preprints are preliminary reports that have not undergone peer review.
They should not be considered conclusive, used to inform clinical practice,
or referenced by the media as validated information.

Spontaneous ignition of vertically oriented wood exposed to convection and time-dependent thermal radiation: experimental and analytical prediction

Li Yan
University of Science and Technology of China
K.M. Liew
City University of Hong Kong
Lizhong Yang
University of Science and Technology of China
Xiaoyu Ju
ju.xiaoyu@ustc.edu.cn

University of Science and Technology of China

Research Article

Keywords: Wood, Ignition behavior, Ignition time prediction, Transient irradiation, Crosswind

Posted Date: May 15th, 2026

DOI: https://doi.org/10.21203/rs.3.rs-9484483/v1

License: This work is licensed under a Creative Commons Attribution 4.0 International License.
Read Full License

Additional Declarations: No competing interests reported.

Spontaneous ignition of vertically oriented wood exposed to convection and time-dependent thermal radiation: experimental and analytical prediction

Abstract

Spontaneous ignition of vertically oriented structural timber induced by transient heat flux and crosswind, which represents a prevalent incident in building fire scenarios, has received little attention in existing studies. This study utilized a self-designed experimental setup, employing five quadratic heat fluxes ($\dot{q}''_{ex} = at^2$, heat flux increasing rates (a): 0.10, 0.13, 0.18, 0.28, 0.40 W/m^{2}s^2) and five crosswind conditions (U_∞ = 0, 0.4, 0.8, 1.0, 1.2 m/s) to systematically investigate timber ignition characteristics under coupled transient thermal radiation and convection. Surface temperature, mass loss rate (MLR) and ignition time were measured and analyzed. Analytical solutions for transient surface temperature were derived via one-dimensional heat conduction theory and validated against the experimental data. Using the critical mass loss rate (13 g/m^{2}s) as the ignition criterion, this study developed ignition time prediction methods applicable to time-dependent thermal radiation scenarios. Results indicate that both surface temperature and MLR are mainly driven by thermal radiation. The approximate solution for the surface temperature is more accurate than the asymptotic solution. An increase in heat flux increasing rate reduces ignition time by an average of 17.4%, while an increase in crosswind speed prolongs ignition time by an average of 3.9%. The theoretical model considering surface heat loss restricts ignition time prediction error to within 20%.

Keywords: Wood; Ignition behavior; Ignition time prediction; Transient irradiation; Crosswind

1. Introduction

Wood is widely used in engineering construction and building decoration owing to its merits of renewability, recyclability and ready availability. However, as a typical

combustible material, its ignition upon heating constitutes the incipient stage of building fires. Extensive studies have been conducted on ignition mechanisms, and diverse reliable ignition prediction models have been established. Cohen [1] installed heat flux gauges on a timber wall and found that the flame thermal radiation received by the wall increases with time as a crown fire advances. This phenomenon has rendered the ignition behavior of solid combustibles under transient thermal radiation, research focuses for numerous scholars. To realize ignition prediction, researchers have adopted a gas-solid phase decoupling strategy, neglected the solid-phase pyrolysis process, and proposed a series of prediction models based on single or composite ignition criteria (e.g., critical surface temperature, critical mass loss rate, critical energy). Yang [2] experimentally investigated the pyrolysis and ignition characteristics of two wood species under linearly increasing heat flux conditions, obtained the numerical solution of surface temperature via an integral model, and proposed a composite ignition criterion combining surface temperature and critical heat flux. Ji et al. [3] further derived an ignition time model based on critical surface temperature. Zhai [4] explored the pyrolysis and spontaneous ignition characteristics of pine wood under linear and quadratic heat fluxes, concluding that the critical mass loss rate is more suitable as an ignition criterion than the critical surface temperature, since the former is less susceptible to heating conditions. Reszka [5] derived analytical expressions for ignition time with respect to critical heat flux and critical surface temperature, which are applicable to linear thermal radiation conditions (with or without surface heat loss). Gong [6] established a transient mass loss analytical model suitable for exponentially increasing heat flux conditions based on Lautenberger's work [7], predicted ignition time using the critical mass loss rate as the ignition criterion, and validated the model efficacy against experimental data obtained from PMMA and pine wood. Previous studies have also investigated other heat flux profiles, such as polynomial [8], fourth-order [9], parabolic [10, 11], and periodic [12] heat fluxes. In addition, certain composite ignition criteria [10, 13], such as the combination of critical surface

temperature and critical mass flux, have been verified to demonstrate favorable applicability.

Wind-aided fire spread is a prevalent occurrence in catastrophic fires, exemplified by the Wang Fuk Court large-scale building fire in Hong Kong and the massive wildfire in Los Angeles. Dry weather and strong winds are both key contributing factors to fire spread and expansion. Previous studies have demonstrated that when wind interacts with smoldering combustibles, the probability of smoldering transitioning to flaming combustion first rises with increasing wind speed [14]. However, once the wind speed exceeds a critical value, the blow-off effect induces smoldering extinguishment [15, 16]. A common feature of these studies is that the ignition source or radiation source is removed once the combustible enters the smoldering stage, with only wind governing the smoldering process via convective effects. Bilbao [17] revealed the competitive mechanism between thermal radiation and convection: constant thermal radiation enhances solid heat transfer, whereas wind impedes heat transfer by cooling the solid boundary. Nevertheless, preliminary research by Yan [18] identified that wind exerts a dual effect on ignition, namely promoting ignition at low wind speeds. Notably, the aforementioned studies on the coupling of thermal radiation and crosswind were all conducted under constant thermal radiation.

A core limitation of the above studies is that the tested samples were all horizontally positioned, and their conclusions are mostly applicable to horizontal combustible such as roofs and floors. However, vertical combustibles also account for a substantial proportion in buildings, including exterior wall structural or decorative materials and scaffolding. Most studies on the ignition behavior of vertical combustibles have been performed under constant thermal radiation [19-21], measuring characteristic parameters including ignition time, mass loss rate, surface temperature and heat release rate. Comparisons with horizontal configurations have revealed that vertical combustibles generally exhibit longer ignition times, with Qie's work [22] representing the sole exception. Studies under transient heating conditions are relatively

scarce. Gong explored the ignition characteristics of vertical PMMA [23] and wood [24] under power-law thermal radiation, confirming that both critical surface temperature and critical mass loss rate are suitable as ignition criteria for such conditions.

Compared with horizontal combustibles, the uniqueness of vertical combustible ignition originates from the enhanced air entrainment induced by their structural configuration, which significantly intensifies convective effects. Particularly under forced convection conditions, the boundary layer adjacent to the combustible surface may be distorted, thereby giving rise to distinctive ignition behavior laws. However, to the best of the authors' knowledge, no study has systematically elucidated the pyrolysis and ignition mechanisms of vertical charring materials under the coupled effects of convection and transient heating. To address this research gap, auto-ignition tests of vertical wood exposed to quadratic heat fluxes and crosswind, a typical scenario in wildland and building fires, are experimentally conducted in this study. The uniformity of surface temperature, which is affected by the boundary layer effect, is analyzed by comparing surface temperatures at three distinct heights along the wood specimen. A solid-phase analytical model is developed to predict transient surface temperature during wood pyrolysis, and model validation is performed through comparison with experimental results. Meanwhile, key parameters including ignition time, critical surface temperature and critical mass loss rate are acquired to clarify the governing mechanism of wood auto-ignition. Finally, an ignition prediction model is constructed based on the determined ignition criterion.

2. Experiment details

2.1 Materials

Pine wood was selected as the research material, and the samples were processed into square specimens measuring 10 cm in side length and 2 cm in thickness. The specimen surfaces were polished to be smooth and burr-free, with no defects such as cracks and knots, and the wood grain was perpendicular to the incident direction of

thermal radiation. To eliminate interference from variations in moisture content, all specimens were dried in an oven at a constant temperature of 80 ℃ for 48 hours prior to the experiment, with their moisture content reaching approximately 4% post-drying. The dried specimens were hermetically sealed and tested within three days to maintain moisture content stability. To simplify the heat transfer process, a one-dimensional heat transfer assumption was employed in this study. During the test, the dried specimens were placed in customized fiber cement containers, with only the upper surface exposed to incident thermal radiation and all other surfaces shielded.

2.2 Experimental setup

An experimental setup capable of generating crosswind and diverse time-dependent thermal radiation was employed to perform the spontaneous ignition tests of wood, as illustrated in Fig. 1. The setup heats vertically oriented specimens. Fig. 1 (a) displays the side view of the apparatus, while Fig. 1 (b) illustrates its front view. As depicted in the figures, the apparatus mainly comprises three components: a radiant heating module, a wind tunnel, and a sample lifting platform. Notably, as the radiant heat source is positioned parallel to the specimen, it is omitted from Fig. 1 (b) to clearly visualize the between wind tunnel airflow and the specimen. The radiant heating module consists of nine silicon carbide rods and a water-cooled tank. The silicon carbide rods are connected to a control system and regulated by a power controller, and the thermal radiation intensity precisely modulated by adjusting the voltage applied across the rods. The water-cooled tank is connected to a tap water supply to enable continuous internal water circulation, which rapidly dissipates heat accumulated in the heat source and eliminates discrepancies between the actual and preset heat flux values induced by heat accumulation. The wind tunnel supplies the forced convection required for the experiments. A glass duct fabricated from three high-temperature-resistant glass panels is installed at the wind tunnel outlet (marked as the blue region in Fig. 1 (b)), which stably directs airflow toward the specimen surface. The sample lifting platform is actuated by a servo motor to satisfy height adjustment requirements for different

experimental conditions, and an electronic balance with an accuracy of 0.01 g is installed on the platform to continuously monitor the specimen mass. To protect the balance from thermal damaged caused by the radiant heat source and specimen ignition, a fireproof plate is installed above the balance for thermal shielding. The specimen is mounted vertically on the fireproof plate, with the gap between its surface and the silicon carbide rods fixed at 10 cm.

Three 0.5-mm type K thermocouples were affixed along the vertical centerline of the exposed wood surface: one positioned at the center, with the remaining two located 2.5 cm from the top and bottom edges, respectively. During testing, the thermocouples may detach or exhibit minor vibrations under crosswind conditions. To eliminate the interference of these factors with mass measurements, temperature and mass were recorded independently.

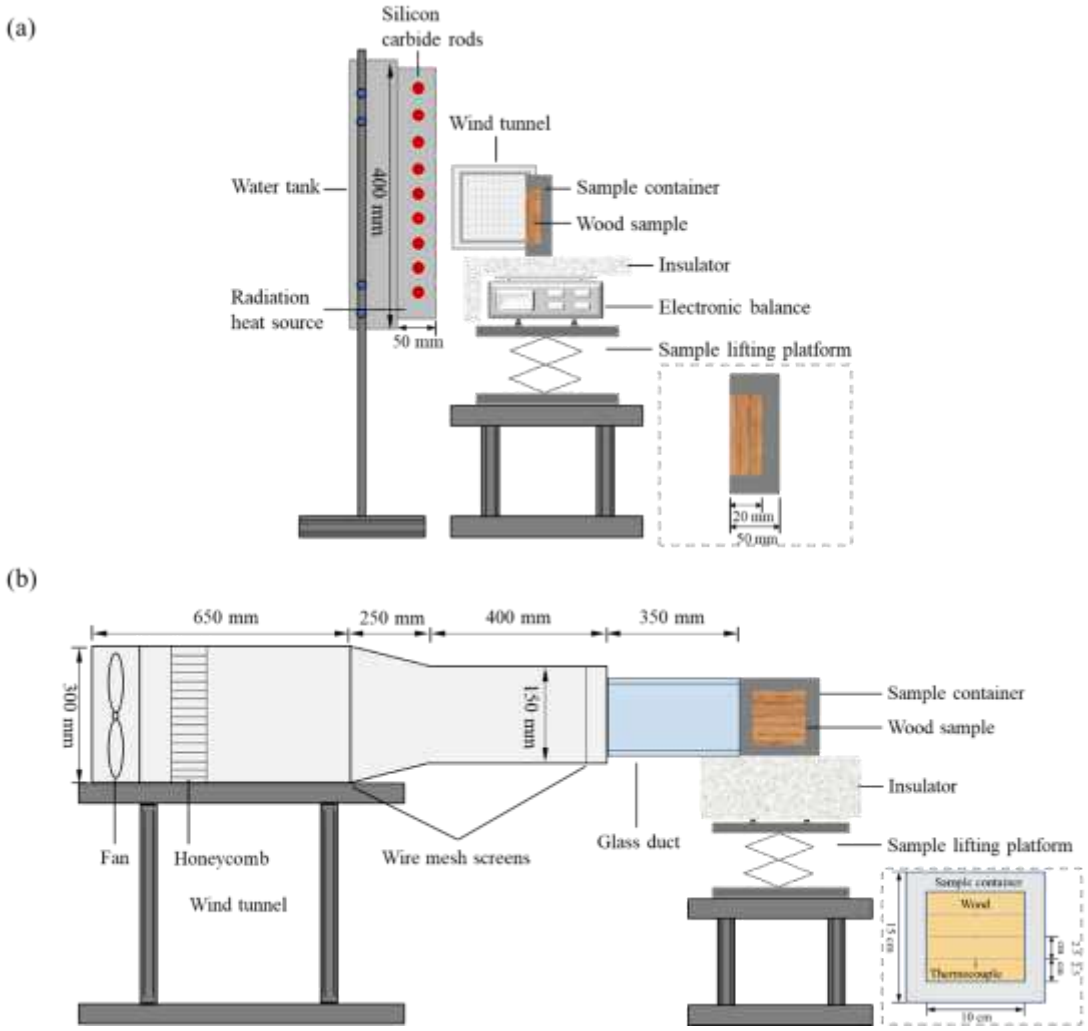


Fig. 1 Schematic configuration of experimental setup **(a)** side view; **(b)** front view

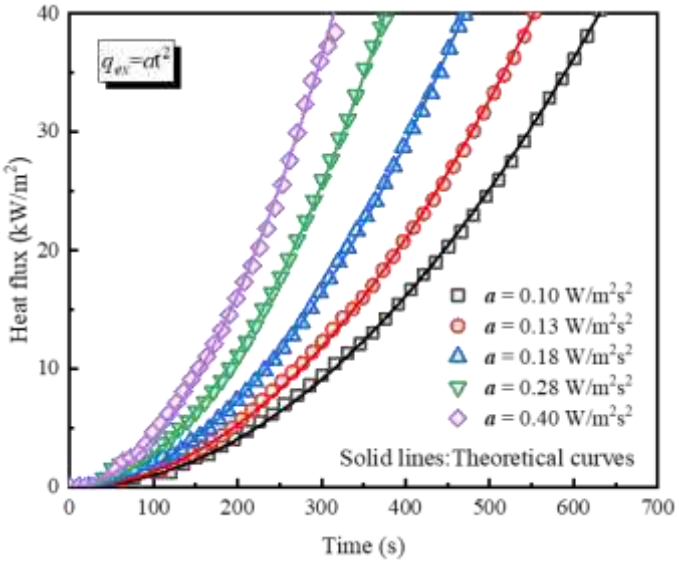
2.3 Crosswind speed and radiant heat flux calibrations

Five designed quadratic heat fluxes were generated by programming the power controller, as expressed by Eq. (1):

$$\dot{q}''_{ex} = at^2 \tag{1}$$

where $\dot{q}''_{ex}$ represents the transient heat flux, t is time, a denotes the rate coefficient that governs the heat flux ramp rate. The peak value of $\dot{q}''_{ex}$ was set to 40 kW/m^2, and the heating program terminated automatically once the thermal radiation attained this peak.

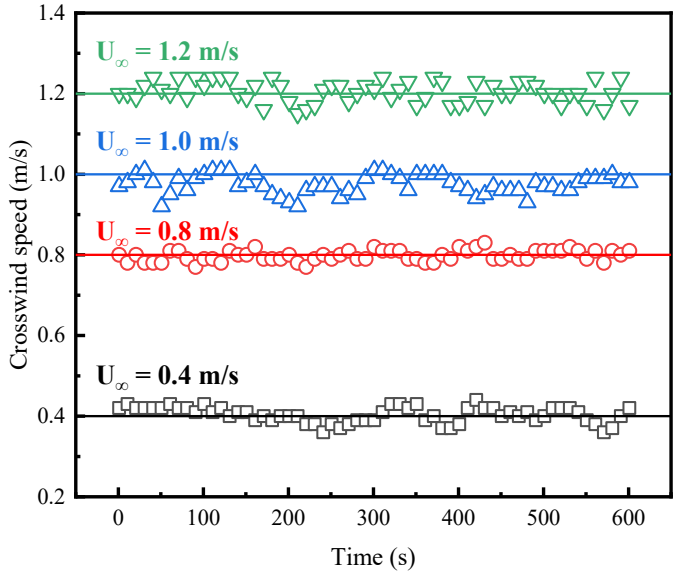
Calibration of the radiant heat flux was performed using a water-cooled radiant heat flux gauge (Model: GTT-25-100-RWF, measurement range of 0–100 kW/m^2, repeatability: ±0.5%, accuracy: ±3%). During calibration, the heat flux gauge was positioned horizontally 10 cm away from the silicon carbide rods, at the same height as the specimen. The calibration comprised two phases: a learning phase and an output phase. In the learning phase, the target heat flux curve was programmed into the control system, which automatically discretized the curve. Upon initiation of the heating program, the system automatically compared the actual heat flux measured by the gauge with the target value, adjusted the two to match via PID control, and synchronously recorded the voltage applied across the silicon carbide rods throughout this process. In the output phase, the system applied the voltages recorded in the learning phase to the silicon carbide rods to generate the target heat flux. As illustrated in Fig. 2, the relative error between the output and target values was below 10%. To validate the spatial uniformity of the heat flux, heat flux gauges were installed along the specimen's central axis (at the center, and 2.5 cm above and below the central point), with the measured discrepancy below 7%.



177

178 **Fig. 2** Time-dependent heat fluxes calibration

179 Four constant crosswind speeds, 0.4, 0.8, 1.0, 1.2 m/s, were adopted based on
180 relevant literature. During crosswind speed calibration, the probe of a hot-wire
181 anemometer (Model: KANOMAX 6243, probe: 0963-00) was affixed near the wood
182 surface, positioned 5 mm horizontally from the surface and aligned with the specimen's
183 central height. The target wind speed was attained by adjusting the fan rotational speed.
184 Each crosswind speed was measured continuously for ten minutes, and the arithmetic
185 mean was adopted as the representative wind speed. The calibration results are
186 presented in Fig. 3.



187

Fig. 3 Crosswind speeds calibration

Experiments were conducted immediately following calibration. A camera (SONY FDR-AX700) was installed to fully record the entire experimental procedure. After the heat source cooled to ambient temperature, the preprocessed specimen was rapidly placed on the fireproof plate, and the gap between its surface and the heat source was adjusted to the preset value (10 cm). Subsequently, the heating program and fan were activated, with the data acquisition system initiated simultaneously at a sampling frequency of 1s. Each test was repeated at least six times, three replicates for surface temperature measurement and three for mass loss collection, to mitigate experimental uncertainties.

3. Theoretical analysis

When wood is exposed to the heat source, its surface absorbs heat, and pyrolysis initiates once the temperature reaches the critical value. The pyrolysis temperature of most solids ranges from 300 to 600 ℃, at which re-radiative heat loss dominates the pyrolysis process [25]. In this study, owing to the presence of forced convection, convective heat loss also cannot be neglected. Assuming that the thermophysical properties of the material are temperature-independent, the preheating process of a thermally thick solid can be described using the classical integral equation for surface temperature evolution [26]：

$$\theta(0,\tau) = \int_0^{\tau} \frac{\tilde{\tau}^b - \lambda_c\theta - \lambda_r[(1+\theta)^4-1]}{\sqrt{\tau-\tilde{\tau}}} d\tilde{\tau} \quad (2)$$

This equation is derived from the one-dimensional heat conduction equation, which accounts only for surface absorption. To simplify the derivation, dimensionless parameters are introduced. Here, θ, τ, $\tilde{\tau}$ represent the dimensionless temperature, dimensionless time and integral variable, respectively. The following dimensionless groups are defined:

$$\theta = \frac{T_s - T_\infty}{T_\infty},\ \tau = \frac{t}{t_r},\ \tilde{\tau} = \frac{\tilde{t}}{t_r} \tag{3}$$

where T_s denotes the transient surface temperature (K), T_∞ is the ambient temperature (K), t_r represents a reference time, $\tilde{t}$ is the integral variable.

Similarly, the following parameters are defined:

$$\lambda_c = \frac{h_{conv} T_\infty}{a t_r^b},\ \lambda_r = \frac{\varepsilon \sigma T_\infty^4}{a t_r^b} \tag{4}$$

where h_{conv} is convective coefficient (W/m^{2}K), σ is the Stefan-Boltzmann constant (W/m^{2}K^4), ε is the surface absorptivity which is assumed to equal the surface emissivity according to Kirchhoff's law [27].

Following simplification and derivation, an asymptotic solution and an approximate solution are obtained:

$$\theta(0,\tau) = \frac{2\beta_1 \tau^{b+0.5}}{1+2\tau^{0.5}(\lambda_c \beta_2 + \lambda_r \beta_3)} \tag{5}$$

$$\theta(0,\tau) = \frac{2\beta_1 \tau^{b+0.5}}{1+2\tau^{0.5}(\lambda_c \beta_2 + \lambda_r \beta_3')} \tag{6}$$

where β_i (i = 1,2,3) is constant:

$$\beta_1 = \int_0^1 (1-\omega^2)^b d\omega,\ \omega = \frac{\sqrt{\pi}}{2}\frac{\Gamma(b+1)}{\Gamma(b+1.5)} \tag{7}$$

where Γ is the Gamma function.

$$\beta_2 = \int_0^1 (1-\omega^2)^{b+0.5} d\omega = \frac{\sqrt{\pi}}{2}\frac{\Gamma(b+1.5)}{\Gamma(b+2)} \tag{8}$$

$$\beta_3 = 2\sqrt{\pi}\left[2\beta_1^3 \frac{\Gamma(4b+3)}{\Gamma(4b+3.5)}\tau^{3b+1.5} + 4\beta_1^2 \frac{\Gamma(3b+2.5)}{\Gamma(3b+3)}\tau^{2b+1} + 3\beta_1 \frac{\Gamma(2b+2)}{\Gamma(2b+2.5)}\tau^{b+0.5} + \frac{\Gamma(b+1.5)}{\Gamma(b+2)}\right] \tag{9}$$

$$\beta_3' = 2\sqrt{\pi}\left[(2.1-0.5b)\tau^{1.2b+0.5} + \frac{\Gamma(b+1.5)}{\Gamma(b+2)}\right] \tag{10}$$

4. Results and discussion

4.1 Flaming ignition phenomena

After the heating program was initiated, the wood surface absorbs heat and conducts it inward. Thermal radiation intensity increases gradually from zero. At low heat flux levels, smoldering is initially triggered on the wood surface, where several persistent glowing spots are observed. As thermal radiation intensity intensifies, pyrolysis reactions commence once the internal solid temperature reaches the pyrolysis threshold, releasing pyrolytic volatiles into the gas phase. Based on the final ignition outcome, the experimental phenomena are classified into two categories, with the specific distribution presented in Fig. 4. The abscissa of Fig. 4 represents crosswind speed, while the ordinate denotes the thermal radiation increasing rate. The results indicate that ignition behavior is predominantly governed by the thermal radiation, and shows a weak correlation with crosswind. The blue region in Fig. 4 corresponds to conditions with a low heat flux increasing rate. Under these conditions, the wood surface is heated gradually, leading to slow pyrolysis kinetics and low volatile product concentrations. Furthermore, owing to the crosswind-induced dilution effect, the local volatile concentration in the gas phase rarely reaches the lower flammability limit, thereby preventing flaming ignition. In contrast, the purple region corresponds to conditions with a high heat flux increasing rate. The wood absorbs more energy per unit time, leading to a substantial increase in the pyrolysis rate and a synchronous elevation in pyrolytic volatile emission. Once the volatile concentration attains the flammability limit and the local gas temperature satisfies the ignition criteria, the transition from smoldering to flaming ignition is achieved.

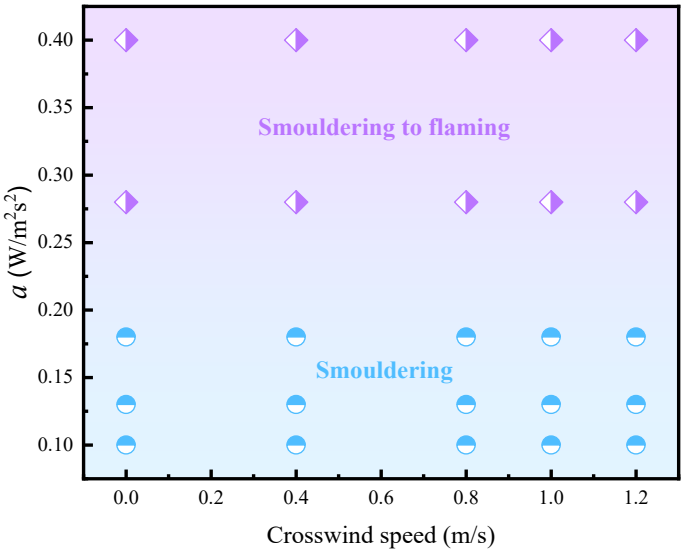


Fig. 4 Zoning diagram of experimental phenomena

This study focuses on the wood ignition process. Fig. 5 presents a representative heat flux case ($\dot{q}''_{ex}$ = 0.28t^2) to illustrate the transition of wood from preheating to ignition under varying crosswind speeds. The abscissa of this figure denotes time, while the ordinate corresponds to crosswind speeds that increase from top to bottom.

From a temporal perspective, the wood surface gradually undergoes charring and cracking upon heating before entering the smoldering stage. Once the critical ignition criteria are met, ignition points first emerge above the sample container and subsequently propagate downward to engulf the entire sample surface. From a convective perspective, the smoke emission from wood during the preheating stage increases substantially with escalating crosswind speed. When $U_\infty \leq$ 0.4 m/s, smoke is primarily distributed in the region above the sample's central height. When 0.8 m/s $\leq U_\infty \leq$ 1.2 m/s, the sample is nearly fully enveloped by smoke.

During the preheating stage, carbon monoxide (CO) and particulate matter produced via char oxidation on the wood surface constitute the primary sources of smoke. Within the smoldering temperature range, hemicellulose and cellulose decompose to generate substantial quantities of volatile organic compounds (VOCs) and tar. Smoldering arises from heterogeneous oxidation reactions between the char layer and oxygen. An increase in crosswind speed accelerates oxygen transport to the

smoldering zone, markedly enhancing the char oxidation reaction rate. The heat released by these oxidation reactions is directly fed back to the wood matrix, sustaining and elevating the temperature of the smoldering zone and further facilitating the pyrolysis of hemicellulose and cellulose. The char layer on the wood surface hinders oxygen diffusion into the wood interior to a certain degree, resulting in an oxygen-deficient state within the specimen. The oxygen deficiency in the smoldering zone inhibits the full oxidation of these pyrolysis products, which are predominately converted into smoke components including soot, polycyclic aromatic hydrocarbons (PAHs), and carbon monoxide, thereby causing smoke emission to rise with escalating crosswind speed. The work of Luca et al. [14] also corroborate that elevated crosswind speeds increase the yields of CO and hydrocarbons (HCs), which supports the trend that smoldering intensity intensifies with increasing crosswind speed.

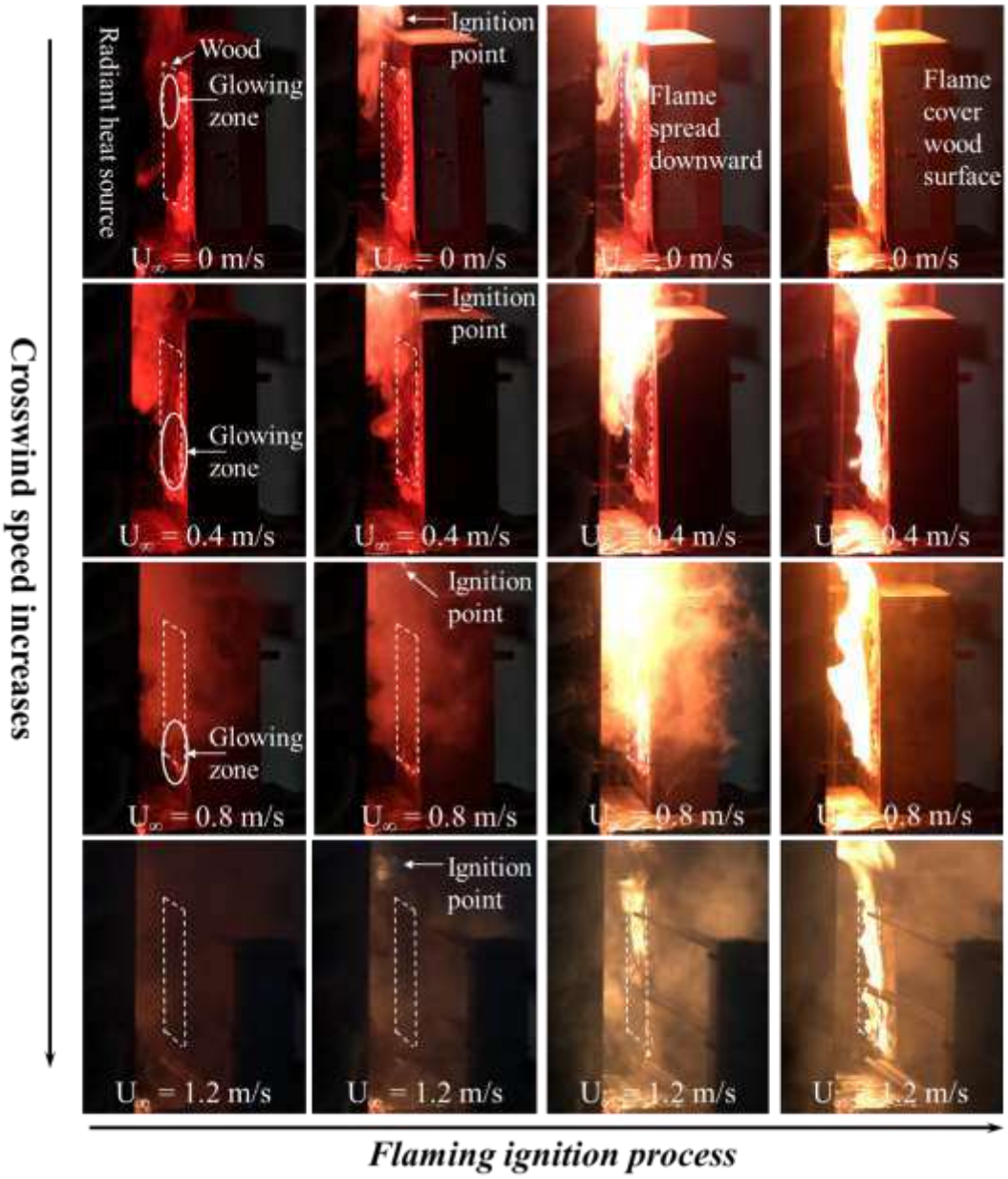


Fig. 5 Flaming ignition phenomena ($\dot{q}''_{ex}$=0.28t^2)

4.2 Surface temperature

Figure 6 presents the surface temperature evolution measured by three thermocouples at different heights of the specimen under diverse heat flux and crosswind speed conditions. The maximum temperature differences for Groups 1, 2, and 3 are less than 3.7%, indicating a uniform surface temperature distribution over the specimen. This trend holds for all other experimental conditions. Accordingly, the surface temperature data utilized in subsequent sections are all obtained from the central

measurement point.

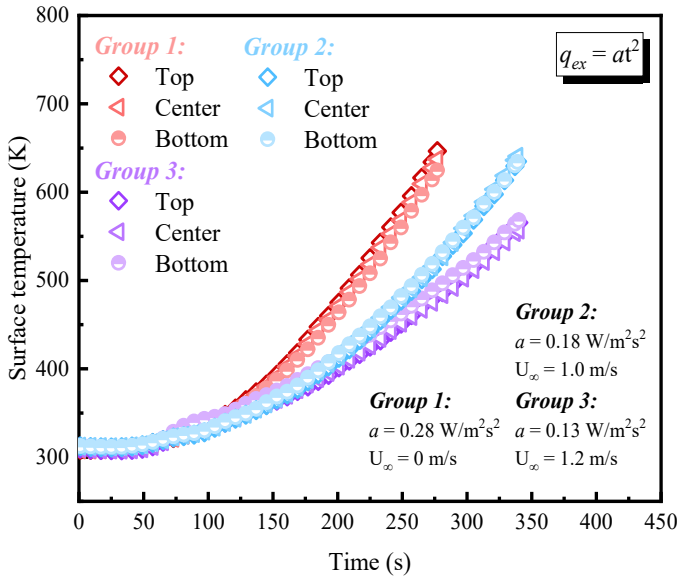


Fig. 6 Measured surface temperature at varying heights

In Fig. 7, the symbols represent the experimentally measured wood surface temperature during the preheating stage, with hollow symbols denoting smoldering conditions and solid symbols representing the smoldering-to-flaming transition conditions. Driven by external time-dependent thermal radiation, the wood surface temperature increases gradually. A higher heat flux increasing rate leads to greater heat absorption per unit time by the wood surface, thereby elevating the surface heating rate. The surface temperature solutions proposed in Section 3 are also validated against experimental data in Fig. 7, where thick solid lines denote the approximate solutions and thin solid lines represent the asymptotic solutions. The average values of λ_c and λ_r are employed for calculations. The results indicate that the approximate solutions can precisely characterize the surface temperature evolution of wood throughout the entire preheating stage. The asymptotic solutions correlate well with experimental data under rapidly increasing heat flux conditions. However, under slowly increasing heat flux conditions, the deviation between the asymptotic solutions and experimental data widens gradually starting from the mid-to-late preheating stage. In particular, during the late preheating stage, the asymptotic solutions tend to plateau, substantially

underestimating the surface temperature. The theoretical surface temperature solutions are derived based on the one-dimensional heat conduction model, which neglects wood pyrolysis and surface char oxidation and assumes the material to be thermally inert. When the thermal radiation increases slowly, the wood experiences a prolonged preheating duration prior to ignition, during which wood pyrolysis becomes non-negligible. In addition, the surface char layer cracks under the combined effects of internal and external temperature gradients and stress disparities, allowing thermal radiation to penetrate the wood interior more readily through these cracks and altering the inherent internal heat conduction process. These factors collectively account for the inevitable deviation between experimental results and theoretical solutions.

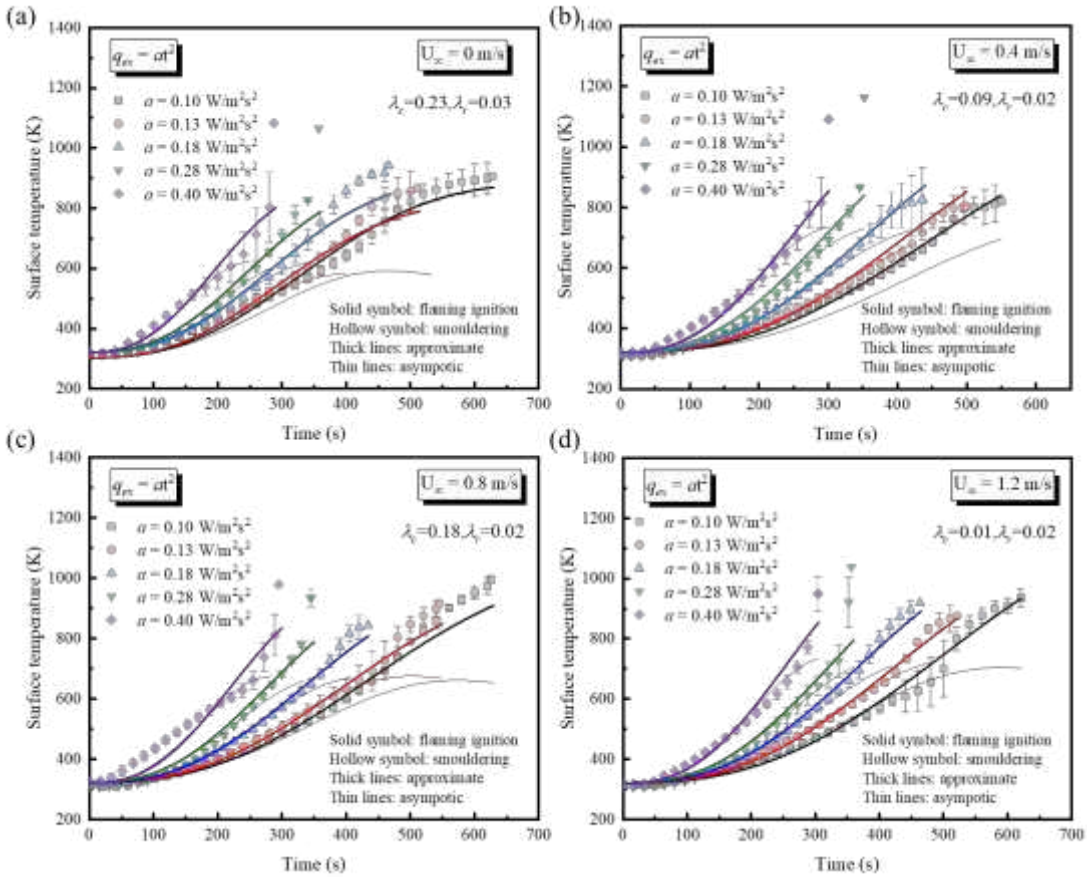


Fig. 7 Measured surface temperature of wood with effect of heat flux and their comparison with analytical solutions

The influence of crosswind on surface temperature is illustrated in Fig. 8, with Fig.

8 (a) and Fig. 8 (b) corresponding to smoldering and smoldering-to-flaming transition conditions, respectively. It can be observed that crosswind exerts a weak regulatory effect on surface temperature under both conditions. The surface temperature trends for other unshown conditions are consistent with the those presented in the figure. For smoldering scenarios, the wood surface temperature in a quiescent environment is slightly higher than that under forced convection, while an increasing crosswind speed does not produce a pronounced variation in the surface temperature history. For the smoldering-to-flaming transition, the surface temperature decreases notably only when $U_\infty \geq$ 1.0 m/s, whereas the surface temperatures under other crosswind conditions are generally comparable. Three key factors govern the wood surface temperature: (1) external thermal radiation, (2) heat release from char oxidation on the wood surface, and (3) surface convective cooling induced by crosswind. Under an identical heat flux, the heat absorbed by the wood surface from the radiation source remains unchanged. Thus, the discrepancies in surface temperature are jointly determined by the latter two factors. An increase in crosswind speed not only cools the surface via convective heat dissipation but also continuously supplies oxygen to the surface, promoting the heterogeneous oxidation reaction and enhancing heat release. Ultimately, the surface temperature is controlled by the competitive balance between convective heat loss and heat generation from char oxidation.

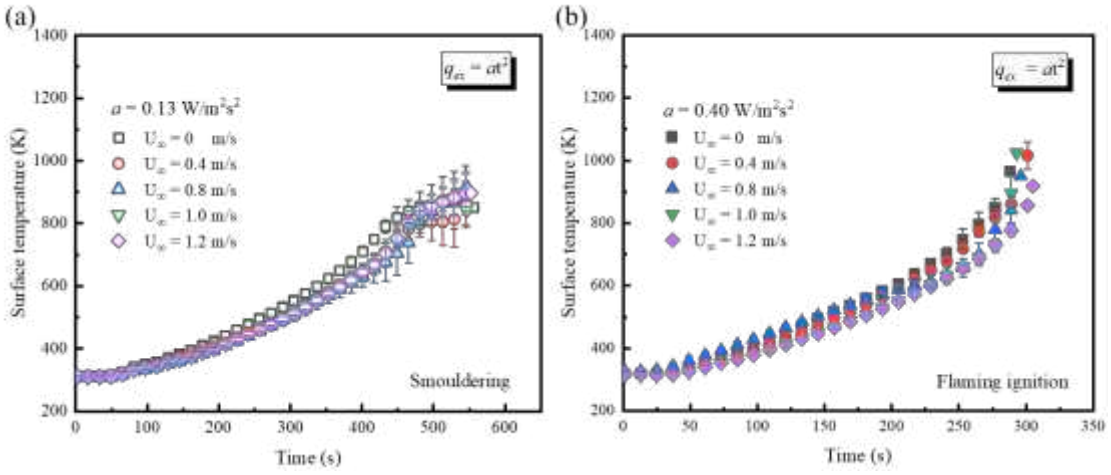
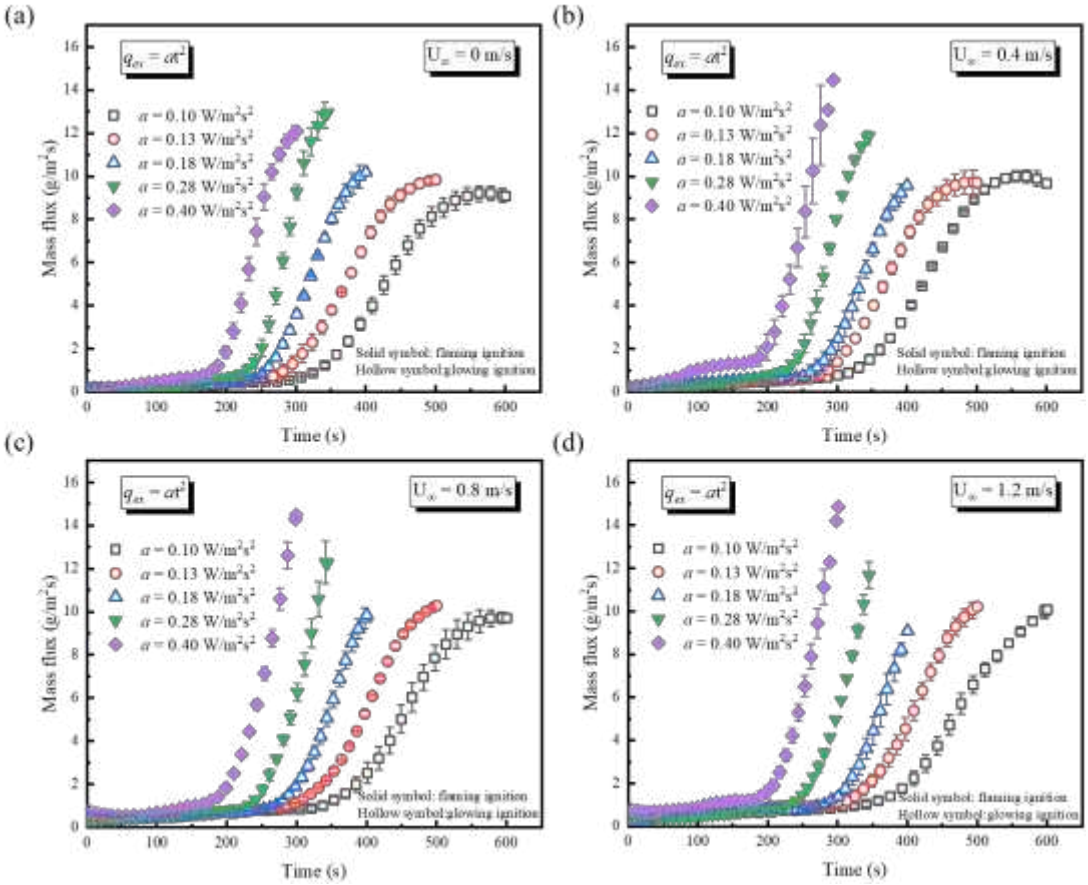


Fig. 8 Measured surface temperature of wood with effect of crosswind speeds

4.3 Mass loss rate

Figure 9 presents the experimental measurements of mass loss rate (MLR), with hollow symbols representing the smoldering regime and solid symbols denoting the smoldering-to-flaming transition regime. As depicted, the wood mass loss process can be divided into two distinct stages: (1) a preheating stage featuring a slowly increasing MLR, (2) a pyrolysis stage characterized by a sharp rise in MLR. A higher heat flux increasing rate leads to an earlier onset of the pyrolysis stage, accompanied by a substantial elevation in MLR during this stage.

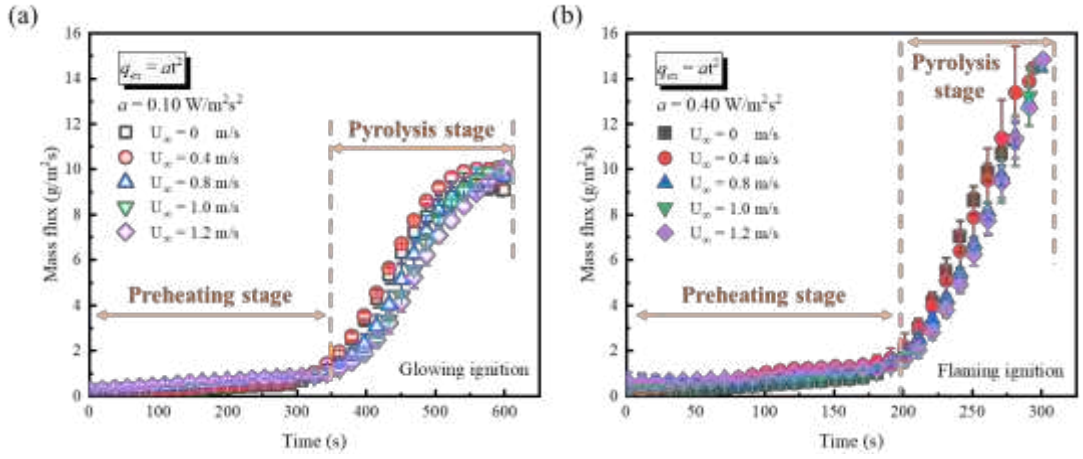
Figure 10 illustrates the effect of crosswind on the wood MLR, where Fig. 10 (a) corresponds to the smoldering regime and Fig. 10 (b) corresponds to the smoldering-to-flaming transition regime. It is evident that the MLR curves under different crosswind speeds are closely clustered, indicating that crosswind exerts a weak regulatory effect on the wood MLR. Regardless of smoldering or ignition, the MLR remain generally consistent when $U_\infty \leq 0.4$ m/s. When $U_\infty \geq 0.8$ m/s, the MLR also tend to be uniform, showing no pronounced variation with further increases in crosswind speed.



366

367 **Fig. 9** Measured mass loss rate of wood with effect of heat flux and their comparison with

368 analytical solutions



369

370 **Fig. 10** Measured mass loss rate of wood with effect of crosswind speeds

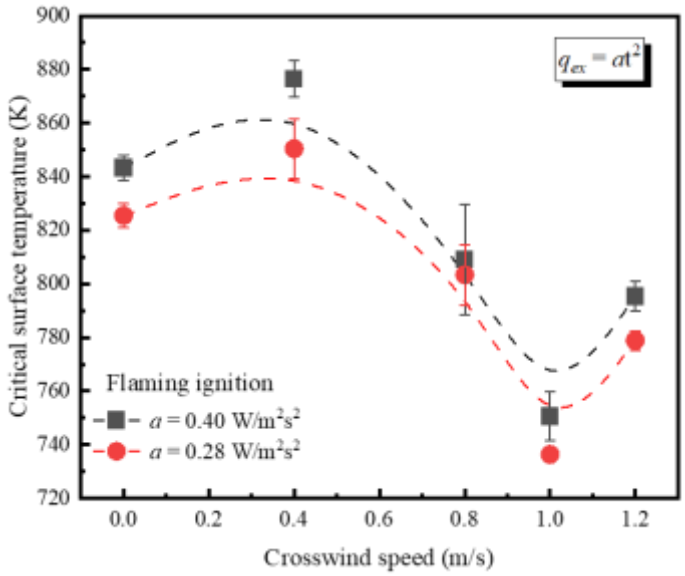
371 **4.4 Flaming ignition criteria**

372 Critical surface temperature and critical mass loss rate represent the two most

widely adopted ignition criteria. A fixed critical value is typically assumed for each criterion, and substituting such values into numerical or analytical models enables the prediction of ignition time. For the smoldering-to-flaming transition investigated in this study, the corresponding critical ignition parameters were measured, laying a foundation for the subsequent development of ignition prediction models.

4.4.1 Critical surface temperature

Figure 11 presents the experimental results of the critical surface temperature, which is defined in this work as the wood surface temperature at the moment of ignition. The results demonstrate a positive correlation between the heat flux increasing rate and the critical surface temperature: a higher heat flux increasing rate corresponds to a greater critical surface temperature. This is because a higher heat flux increasing rate implies a greater thermal energy absorption by the wood surface per unit time, which directly results in a higher surface temperature. Meanwhile, the elevated surface temperature promotes heterogeneous oxidation reactions and enhances heat generation, forming a positive feedback loop that further elevates the surface temperature. With an increase in crosswind speed, the critical surface temperature exhibits an overall downward trend, indicating that the increment in convective heat dissipation surpasses that in heat release from char oxidation, once the crosswind speed reaches a threshold value. Consequently, convective heat dissipation becomes the dominant factor governing the critical surface temperature. The fluctuation range of the critical surface temperature induced by crosswind is more than 100 K, verifying that the critical surface temperature is significantly influenced by convection.



396

397 **Fig. 11** Measured critical surface temperature

398 *4.4.2 Critical mass loss rate*

399 The critical mass loss rate can reflect the lower flammability limit concentration
400 of pyrolytic volatiles in the gas phase. Figure 12 presents the experimentally measured
401 critical MLR of wood at the moment of ignition. The critical MLR fluctuates irregularly
402 with varying crosswind speeds, and under crosswind conditions, a higher heat flux
403 increasing rate corresponds to larger critical MLR values. Notably, the critical MLR
404 fluctuates only within a narrow range of 12–14 kg/m^{2}s across all tests, indicating that
405 it is essentially insensitive to thermal radiation and crosswind. In this study, the average
406 value of experimental critical MLR data under ignition conditions, i.e., 13 kg/m^{2}s, is
407 adopted as the characteristic value.

408 Previous research [28] has indicated that the critical MLR is directly correlated
409 with the lower flammability limit of the volatile-air mixture, a property that makes it a
410 more reliable ignition criterion than the critical surface temperature. Combined with the
411 favorable stability of the critical MLR observed in this study, it can be concluded that
412 the critical MLR serves as a more robust ignition criterion under the coupled conditions
413 of transient thermal radiation and crosswind. Approximate solutions for ignition time
414 will be derived based on this criterion in Section 4.5.

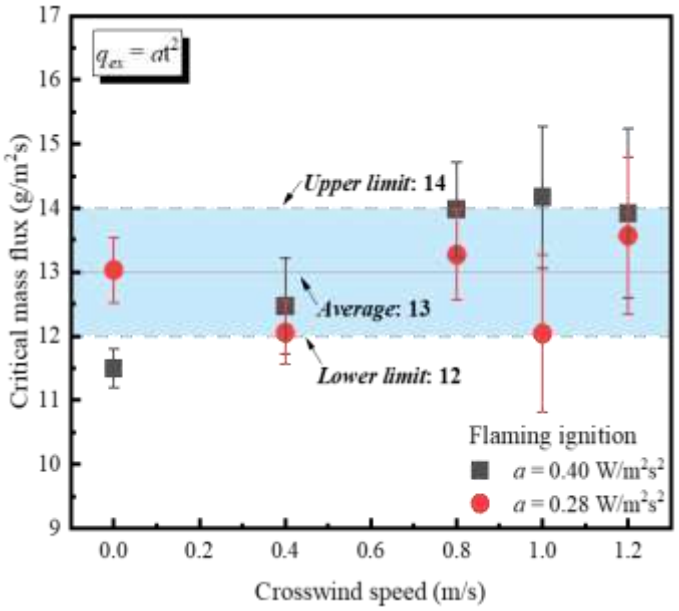
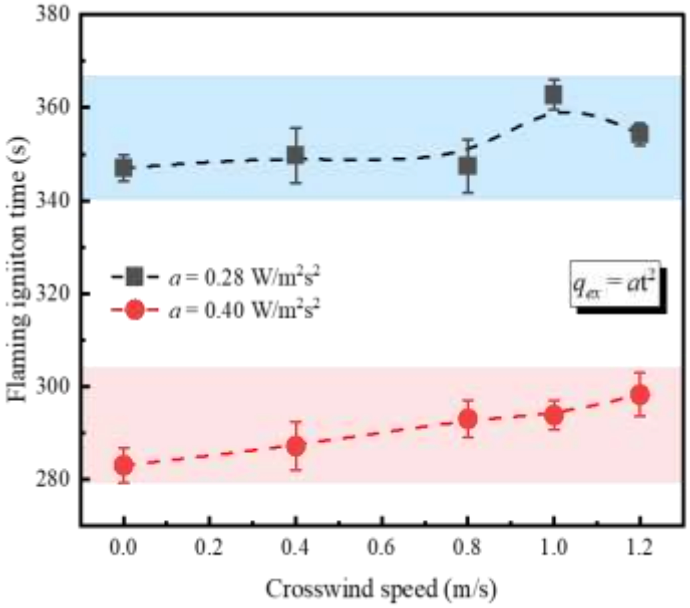


Fig. 12 Measured critical mass loss rate

4.5 Flaming ignition time

4.5.1 Experimental results

Figure 13 presents the experimental results of flaming ignition time. The blue region illustrates the variations in ignition time with crosswind speed at a heat flux increasing rate of 0.28 W/m^{2}s^2 (ignition times ranged from 347 to 363 s.), while the pink region corresponds to the condition with a heat flux increasing rate of 0.40 W/m^{2}s^2 (ignition times ranged from 283 to 299 s.). As the radiant heat flux increases faster, ignition time decreases by 17.6%–18.4% across all crosswind speeds. The results demonstrate that a higher heat flux increasing increase significantly shortens the ignition time: under this condition, the wood surface heats up rapidly, intense pyrolysis reactions occur within the thin layer, and the release rate of flammable pyrolytic volatiles into the gas phase is accelerated, allowing the volatiles to reach the lower flammability limit within a short duration. As crosswind speed increases, ignition time exhibits a slight increasing trend. Under the two radiant heat flux conditions, ignition time increases by 4.6% and 5.7%, respectively. This is attributed to the combined effects of surface convective cooling and flammable volatile dilution.



433

434 **Fig. 13** Measured flaming ignition time

435 Ignition time is a key parameter in fire safety research, and its accurate prediction
436 offers critical guidance for fire prevention and mitigation. Based on the conclusions
437 presented in Section 4.4, this study establishes a correlation between ignition time and
438 critical mass loss rate. Two ignition time prediction methods are proposed in this work,
439 which extend the models developed by previous studies for constant thermal radiation
440 to transient thermal radiation scenarios.

441 *4.5.2 Approximate solution without surface heat loss*

442 Flaming ignition is assumed to occur once the critical mass loss rate is attained,
443 and the gas-phase induction time is assumed to be invariant and sufficiently short
444 relative to the heating time. By substituting the Arrhenius pyrolysis rate with a power-
445 law dependence, a closed-form approximation was developed to estimate the transient
446 mass loss rate. Subsequently, an explicit closed-form approximate solution for ignition
447 time of a semi-infinite solid irradiated by constant heat flux in the absence of surface
448 heat loss was derived using the critical mass loss rate as the ignition criterion [7]:

449 $$\sqrt{t_{ig}} = \sqrt{\frac{\pi}{4} k\rho C_p} \frac{T_{ig}^* - T_\infty}{\dot{q}_{ex}''} \quad (11)$$

$$T_{ig}^{*} = T_{\infty}\left[\frac{T_{ac}^{v}\cdot \dot{q}_{ex}''\cdot \dot{m}_{ig}''}{k\rho u A_p \cdot T_{\infty}\cdot exp(-T_{ac}/T_1)}\right]^{T_2/T_{ac}} \quad (12)$$

where t_{ig} represents the ignition time (s), k and ρ are the thermal conductivity (W/m·K) and density (kg/m^3) of wood, T_{ac} is the activation temperature, defined as the activation energy divided by the universal gas constant, $T_{ac} = E_a/R$, $\dot{m}_{ig}''$ is the critical mass loss rate (kg/m^3), u is a constant,, A_p is the pre-exponential factor (s^{-1}), T_1 and T_2 are constants.

It can be inferred from Eq. (1) that at ignition:

$$\dot{q}_{ex}'' = at_{ig}^2 \quad (13)$$

Substituting Eq. (13) into Eq. (12) to eliminate $\dot{q}_{ex}''$ yields：

$$T_{ig}^{*} = T_{\infty}\left[\frac{T_{ac}^{v}\cdot at_{ig}^2\cdot \dot{m}_{ig}''}{k\rho u A_p \cdot T_{\infty}\cdot exp(-T_{ac}/T_1)}\right]^{T_2/T_{ac}} \quad (14)$$

where v is a constant.

Define:

$$K_1 = \frac{T_{ac}^{v}\cdot a\cdot \dot{m}_{ig}''}{k\rho u A_p \cdot T_{\infty}\cdot exp(-T_{ac}/T_1)} \quad (15)$$

Equation (14) is then simplified to:

$$T_{ig}^{*} = T_{\infty}\left(K_1 \cdot t_{ig}^2\right)^{T_2/T_{ac}} \quad (16)$$

After dividing both sides of Eq. (16) by T_{∞}, the T_2/T_{ac}-th power is taken for both sides:

$$\left(T_{ig}^{*}/T_{\infty}\right)^{T_{ac}/2T_2} = \sqrt{K_1}\cdot t_{ig} \quad (17)$$

which gives:

$$t_{ig} = \frac{\left(T_{ig}^{*}/T_{\infty}\right)^{Tac/2T_2}}{\sqrt{K_1}} \quad (18)$$

Substituting K_1 into Equation (18) yields:

$$t_{ig} = \frac{\left(T_{ig}^{*}/T_{\infty}\right)^{T_{ac}/2T_2} \cdot \left[k\rho u A_p \cdot T_{\infty} \cdot exp(-T_{ac}/T_1)\right]^{1/2}}{\left(T_{ac}^{v} \cdot a \cdot \dot{m}_{ig}''\right)^{1/2}} \quad (19)$$

$$K_{total} = \frac{\left(T_{ig}^{*}/T_{\infty}\right)^{T_{ac}/2T_2} \cdot \left[k\rho u A_p \cdot T_{\infty} \cdot exp(-T_{ac}/T_1)\right]^{1/2}}{(T_{ac}^{v} \cdot a)^{1/2}} \quad (20)$$

$$t_{ig} = K_{total} \cdot \frac{1}{\sqrt{\dot{m}_{ig}''}} \quad (21)$$

4.5.3 Approximate solution with convective and radiative heat loss

The classical thermal theory is extended by incorporating two key physical processes: the surface heat balance of the exposed specimen and the finite-rate pyrolysis within the material matrix. For specimens of arbitrary thickness, approximate analytical solutions for the temperature distribution are derived with due consideration given to external radiative heating, surface re-radiation losses, heat of gasification, and convective heat loss. Based on the assumption of the high activation energy limit, the volatile mass loss rate is quantified by integrating the pyrolysis rate throughout the material layer. Subsequently, the ignition time of a solid exposed to constant heat flux, with the critical mass loss rate adopted as the ignition criterion, can be formulated mathematically as [28]:

$$t_{ig} = \frac{\pi}{4} k\rho C_p \left(\frac{T_{ig}-T_{\infty}}{\varepsilon \cdot \dot{q}_{ex}''}\right)^2 \left[1 - C \cdot \frac{h_{eff}(T_{ig}-T_{\infty})}{\varepsilon \cdot \dot{q}_{ex}''}\right]^{-2} \quad (22)$$

$$h_{eff} = \frac{z}{exp(z)-1} \cdot h_{conv} + \frac{\varepsilon\sigma \cdot T_s^4 + L \cdot \dot{m}_{ig}''}{T_s - T_{\infty}} \quad (23)$$

where C is the constant, z is dimensionless mass flux of volatiles, L is the heat of gasification (J/g).

The first-order Taylor approximation of the function $f(x) = (1-x)^{-2}$ is given by:

$$(1-x)^{-2} \approx 1 + 2x \quad (24)$$

$$x = C \cdot \frac{h_{eff}(T_{ig}-T_{\infty})}{\varepsilon \cdot \dot{q}_{ex}''} \quad (25)$$

Substituting Equations (24) and (25) into Eq. (22) gives:

493 $$t_{ig} = \frac{\pi}{4} k\rho C_p \left(\frac{T_{ig}-T_\infty}{\varepsilon \cdot \dot{q}''_{ex}}\right)^2 \cdot \left[1 + 2C \cdot \frac{h_{eff}(T_{ig}-T_\infty)}{\varepsilon \cdot \dot{q}''_{ex}}\right] \quad (26)$$

494 Substituting Eq. (13) into Eq. (26) further yields:

495 $$t_{ig}^5 = \frac{\pi k\rho C_p (T_{ig}-T_\infty)^2}{4\varepsilon^2 a^2} \cdot \left[1 + 2C \cdot \frac{h_{eff}(T_{ig}-T_\infty)}{\varepsilon \cdot a \cdot t_{ig}^2}\right] \quad (27)$$

496 Both sides are multiplied by t_{ig}^2 to eliminate t_{ig}^2 in the denominator on the right-hand
497 side:

498 $$t_{ig}^7 = \frac{\pi k\rho C_p (T_{ig}-T_\infty)^2}{4\varepsilon^2 a^2} \cdot t_{ig}^2 + \frac{\pi k\rho C_p (T_{ig}-T_\infty)^3 \cdot C \cdot h_{eff}}{2\varepsilon^3 a^3} \quad (28)$$

499 Based on the experimental results, t_{ig} > 300 s, and $t_{ig}^2 \ll t_{ig}^7$. Thus, the first term on
500 the right-hand side of the equation can be neglected, and Eq. (28) is simplified to:

501 $$t_{ig}^7 = \frac{\pi k\rho C_p (T_{ig}-T_\infty)^3 \cdot C \cdot h_{eff}}{2\varepsilon^3 a^3} \quad (29)$$

502 $$t_{ig} = \left[\frac{\pi k\rho C_p (T_{ig}-T_\infty)^3 \cdot C}{2\varepsilon^3 a^3} \left(\frac{C_p \cdot \dot{m}''_{ig}}{exp\left(C_p \cdot \dot{m}''_{ig}/h_{conv}\right)-1} + \frac{\varepsilon\sigma \cdot T_{ig}^4 + L \cdot \dot{m}''_{ig}}{T_{ig}-T_\infty}\right)\right]^{1/7} \quad (30)$$

503 The primary parameters utilized in the calculations are presented in Table 1.

504 **Table 1**

505 Values of parameters used in the calculation.

Parameters	Values	Unit	References
v	0.85	[-]	[7]
u	341.3	[-]	[7]
E_a	106.5	kJ/mol	[29]
R	8.314	J/(mol·K)	[30]
k	0.15	W/(m·K)	[29]
ρ	450	kg/m^3	Measured
A_p	5.25×10^7	s^{-1}	[29]
T_1	357	K	[7]
T_2	615	K	[7]
C	0.9	[-]	[28]
ε	0.78	[-]	[31]

506

Figure 14 presents a comparison between the approximate solutions of ignition time obtained by the two aforementioned methods and the experimental results. Method 1, which neglects surface heat loss, yields accurate predictions solely under still air conditions. In contrast, Method 2 incorporates both convective and radiative heat loss, keeping the prediction error within 20% thereby validating the model's applicability to this study.

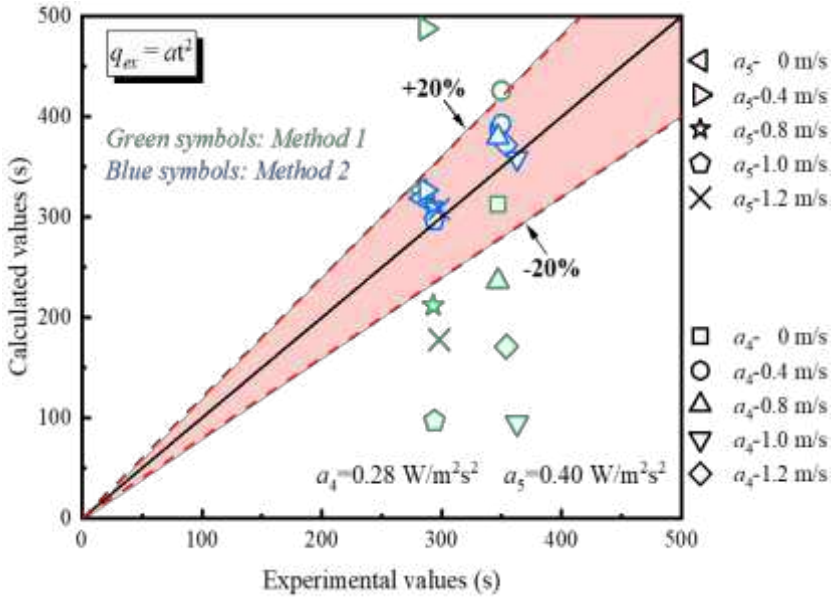


Fig. 14 Comparison of experimental and approximate solutions of flaming ignition time

5. Conclusions

Most previous studies on the spontaneous ignition of wood focused on horizontally oriented specimens and a single heating condition. However, in practical fire scenarios, vertically mounted combustibles such as timber wall panels and fences are very commonly subjected to transient thermal radiation from external fire sources or window spill fires. This study systematically investigates the spontaneous ignition behavior of vertically oriented structural timber under coupled transient thermal radiation and crosswind. Key parameters, including surface temperature, mass loss rate and ignition time, were experimentally measured. A one-dimensional analytical model was developed to predict the transient surface temperature during pyrolysis. Finally, an

ignition prediction model applicable to transient thermal radiation conditions was derived using the critical mass loss rate as the ignition criterion. The main findings are summarized as follows:

(1) Wood ignition modes are categorized into two distinct types (smouldering and smouldering-to-flaming transition), with the heat flux ramp rate being the dominant controlling factor. Flaming ignition of wood occurs only when the thermal radiation increases sufficiently fast (i.e., $a \geq 0.28$ W/m^{2}s^2 in this study). An increase in crosswind speed enhances the smoldering intensity and elevates the content of incompletely oxidized pyrolytic volatiles, thereby significantly elevating smoke production during the wood preheating stage.

(2) Surface temperature is primarily governed by thermal radiation rather than crosswind. An accelerating heat flux increasing rate markedly accelerates surface temperature rise. In contrast, crosswind speed exerts a weak influence on surface temperature. Under identical heat flux conditions, the divergence in surface temperature corresponding to different crosswind speeds arises primarily from the competitive balance between the heat release from char oxidation and convective heat dissipation. The approximate solution derived from the one-dimensional model provides satisfactory predictive accuracy for the transient surface temperature. However, when the thermal radiation increases slowly ($a \leq 0.13$ W/m^{2}s^2), the deviation between the asymptotic solution and experimental results gradually widens from the mid-preheating stage. This deviation primarily stems mainly from the model's neglection of pyrolysis reactions and the temperature dependence of the material's thermophysical properties. Furthermore, the thickening char layer in the late preheating stage impedes heat transfer, further reducing the prediction accuracy.

(3) Wood enters the rapid pyrolysis stage after a preheating period. A slower thermal radiation corresponds to a prolonged preheating stage. Meanwhile, the heat flux increasing rate exhibits a positive correlation with the wood mass loss rate, and a higher rate leads to a greater mass loss rate. Since crosswind speed has a minor effect on

surface temperature, and the mass loss rate is governed by the heat transfer process, its variation is also insensitive to crosswind.

(4) The critical surface temperature and the critical mass loss rate are the two most widely adopted ignition criteria. The experimental results demonstrate that the critical surface temperature is significantly affected by environmental conditions, with a maximum temperature difference of up to 100 K observed across different crosswind speeds. In contrast, the critical mass loss rate is nearly independent of thermal radiation and crosswind, exhibiting superior stability. Therefore, it serves as a more reliable ignition criterion for this study.

(5) A higher heat flux increasing rate significantly shortens the ignition time, whereas an increase in crosswind speed leads to a slight prolongation of ignition time. Using the critical mass loss rate as the ignition criterion, this study proposes two prediction models. The first one yields low predictive accuracy because it neglects surface heat loss. The second one, which incorporates both convective and radiative heat losses, is derived by coupling the specimen's surface heat balance with the integral of the pyrolysis rate over the entire control volume, with its prediction error controlled within 20%.

References

[1] Cohen JD, Relating flame radiation to home ignition using modeling and e xperimental crown fires, Can. J. For. Res. 2004;34: 1616-26. https://doi.org/10.1 139/x04-049

[2] Lizhong Y, Zaifu G, Jingwei J, Weicheng F, Experimental Study on Sponta neous Ignition of Wood Exposed to Variable Heat Flux, J. Fire Sci. 2005;23: 4 05-16.

[3] Ji J, Cheng Y, Yang L, Guo Z, Fan W, An Integral Model for Wood Auto -ignition under Variable Heat Flux, J. Fire Sci. 2006;24: 413-25.

[4] Zhai C, Gong J, Zhou X, Peng F, Yang L, Pyrolysis and spontaneous ignit ion of wood under time-dependent heat flux, J. Anal. Appl. Pyrolysis. 2017;12 5: 100-08. https://doi.org/10.1016/j.jaap.2017.04.013

[5] Reszka P, Borowiec P, Steinhaus T, Torero JL, A methodology for the esti mation of ignition delay times in forest fire modelling, Combust. Flame. 2012; 159: 3652-57. https://doi.org/10.1016/j.combustflame.2012.08.004

[6] Gong J, Li Y, Chen Y, Li J, Wang X, Jiang J, Wang Z, Wang J, Approximate analytical solutions for transient mass flux and ignition time of solid combustibles exposed to time-varying heat flux, Fuel, 2018;211: 676-87. https://doi.org/10.1016/j.fuel.2017.09.107
[7] Lautenberger C, Fernandez-Pello A, Approximate Analytical Solutions For The Transient Mass Loss Rate And Piloted Ignition Time Of A Radiatively Heated Solid In The High Heat Flux Limit, Fire Saf. Sci. 2005;8: 445-56.
[8] Lamorlette A, Analytical modeling of solid material ignition under a radiant heat flux coming from a spreading fire front, J. Therm. Sci. Eng. Appl. 2014;6. https://doi.org/10.1115/1.4028204
[9] DiDomizio MJ, Mulherin P, Weckman EJ, Ignition of wood under time-varying radiant exposures, Fire Saf. J. 2016;82: 131-44. https://doi.org/10.1016/j.firesaf.2016.02.002
[10] Vermesi I, Roenner N, Pironi P, Hadden RM, Rein G, Pyrolysis and ignition of a polymer by transient irradiation, Combust. Flame. 2016;163: 31-41. https://doi.org/10.1016/j.combustflame.2015.08.006
[11] Vermesi I, DiDomizio MJ, Richter F, Weckman EJ, Rein G, Pyrolysis and spontaneous ignition of wood under transient irradiation: Experiments and a-priori predictions, Fire Saf. J. 2017;91: 218-25. https://doi.org/10.1016/j.firesaf.2017.03.081
[12] Fang J, Meng Y-R, Wang J-W, Zhao L-Y, He X-Z, Ji J, Zhang Y-M, Experimental, numerical and theoretical analyses of the ignition of thermally thick PMMA by periodic irradiation, Combust. Flame. 2018;197: 41-48. https://doi.org/10.1016/j.combustflame.2018.07.009
[13] Gong J, Zhang M, Zhai C, Composite auto-ignition criterion for PMMA (Poly methyl methacrylate) exposed to linearly declining thermal radiation, Appl. Therm. Eng. 2021;195: 117156. https://doi.org/10.1016/j.applthermaleng.2021.117156
[14] Carmignani L, Hajilou M, Cobian-Iñiguez J, Finney M, Stephens SL, Goller MJ, Fernandez-Pello C, Smoldering of Wood: Effects of Wind and Fuel Geometry, Fire Technol. 2024;60: 1667-83. https://doi.org/10.1007/s10694-024-01542-8
[15] Lin S, Chow TH, Huang X, Smoldering propagation and blow-off on consolidated fuel under external airflow, Combust. Flame. 2021;234: 111685. https://doi.org/10.1016/j.combustflame.2021.111685
[16] Santoso MA, Christensen EG, Rein G, The effects of pulsating wind on the transition from smouldering to flaming combustion, Fire Saf. J. 2023;141: 103993. https://doi.org/10.1016/j.firesaf.2023.103993
[17] Bilbao R, Mastral JF, Aldea ME, Ceamanos J, Betrán M, Lana JA, Experimental and theoretical study of the ignition and smoldering of wood including convective effects, Combust. Flame. 2001;126: 1363-72. https://doi.org/10.1016/S0010-2180(01)00251-6

627 [18] Yan L, Ju X, Liu H, Gong J, Lai D, Xu J, Yang L, Ignition limits of pi
628 ne wood building material under the coupling effects of thermal radiation and
629 cross winds, J. Build. Eng. 2024;96: 110576. https://doi.org/10.1016/j.jobe.2024.
630 110576
631 [19] Chen X, Zhou Z, Li P, Zhou D, Wang J, Effects of sample orientation o
632 n pyrolysis and piloted ignition of wood, J. Fire Sci. 2014;32: 483-97.
633 [20] Terrei L, Flity H, Ikhou O, Trohel G, Torero JL, Acem Z, Parent G, Effe
634 ct of the wood species on the fire behavior in vertical orientation, Fire Saf. J.
635 2024;148: 104234. https://doi.org/10.1016/j.firesaf.2024.104234
636 [21] Tsai K-C, Orientation effect on cone calorimeter test results to assess fire
637 hazard of materials, J. Hazard. Mater. 2009;172: 763-72. https://doi.org/10.1016/
638 j.jhazmat.2009.07.061
639 [22] Junfang Qie, Lizhong Yang, Yafei Wang, Jiakun Dai, Xiaodong Zhou, Exp
640 erimental Study of the Influences of Orientation and Altitude on Pyrolysis and
641 Ignition of Wood, J. Fire Sci. 2011;29: 243-58. https://doi.org/10.1016/j.jhazmat.
642 2009.07.061
643 [23] Gong J, Zhu Z, Zhang M, Zhai C, Wang X, Piloted ignition of vertical p
644 olymethyl methacrylate (PMMA) exposed to power-law increasing radiation, Ap
645 pl. Therm. Eng. 2022;217: 118996. https://doi.org/10.1016/j.applthermaleng.2022.
646 118996
647 [24] Gong J, Zhang Y, Fang Y, Li L, Huang Y, Glowing and piloted flaming
648 ignition of vertical wood exposed to power-law thermal radiation, J. Build. En
649 g. 2024;84: 108558. https://doi.org/10.1016/j.jobe.2024.108558
650 [25] Delichatsios MA, Chen Y, Asymptotic, approximate, and numerical solutio
651 ns for the heatup and pyrolysis of materials including reradiation losses, Comb
652 ust. Flame. 1993;92: 292-307. https://doi.org/10.1016/0010-2180(93)90041-Z
653 [26] Gong J, Delichatsios MA, Asymptotic and approximate solutions for pilote
654 d ignition of thermally thick solids under power-law heat flux, Fire Saf. J. 202
655 3;141: 103956. https://doi.org/10.1016/j.firesaf.2023.103956
656 [27] Carslaw HS, Jaeger JC, Feshbach H, Conduction of heat in solids, Phys.
657 Today. 1962;15: 74-76. https://doi.org/10.1007/978-1-4939-2565-0_2
658 [28] Snegirev A, Kuznetsov E, Markus E, Coupled analytical approach to predi
659 ct piloted flaming ignition of non-charring polymers, Fire Saf. J. 2017;93: 74-8
660 3. https://doi.org/10.1016/j.firesaf.2017.08.006
661 [29] Kung H-C, A mathematical model of wood pyrolysis, Combust. Flame. 19
662 72;18: 185-95. https://doi.org/10.1016/S0010-2180(72)80134-2
663 [30] Correa N, Cuevas J, Fuentes A, Torero JL, Reszka P, Understanding the e
664 ffect of char oxidation on wood temperature profiles for varying heating and o
665 xygen conditions, Fire Saf. J. 2024;142: 104049. https://doi.org/10.1016/j.firesaf.
666 2023.104049
667 [31] Shen DK, Fang MX, Luo ZY, Cen KF, Modeling pyrolysis of wet wood
668 under external heat flux, Fire Saf. J. 2007;42: 210-17. https://doi.org/10.1016/j.fi

669 resaf.2006.09.001
670